Selective Crystallization of Linkage Isomers, [Rh ^ III(NCS)(SCN)_5] ^ 3- and [Rh ^ III(SCN)_6] ^ 3-, to Investigate Structural Trans Influence and Thermal Stability

Inorganic Chemistry

pubs.acs.org/IC Article

Selective Crystallization of Linkage Isomers, $[Rh^{III}(NCS)(SCN)_5]^{3-}$ and $[Rh^{III}(SCN)_6]^{3-}$, to Investigate Structural Trans Influence and Thermal Stability

Miki Mukai, Seiya Hagiwara, Rika Tanaka, Hiroyasu Tabe, Takashi Nakazono, and Yusuke Yamada*

Cite This: https://doi.org/10.1021/acs.inorgchem.3c02292 Read Online

ACCESS | Metrics & More | Article Recommendations | Supporting Information

ABSTRACT: Linkage isomers of homoleptic complexes, $[Rh^{III}(SCN)_6]^{3-}$ and $[Rh^{III}(NCS)(SCN)_5]^{3-}$, formed in aqueous solution were successfully separated by employing methyltriphenylphosphonium ($MePPh_3^+$) and 1-ethylquinolinium ($EtQu^+$) ions as countercations, respectively. The single-crystal X-ray analysis of $(MePPh_3)_3[Rh^{III}(SCN)_6]$ (**1**) indicated that all of the SCN^- ligands coordinate to the Rh^{III} ion by S atoms with an octahedral symmetry, where the average bond length of Rh−S is 2.374(7) Å. On the other hand, the Rh^{III} ion of $(EtQu)_3[Rh^{III}(NCS)(SCN)_5]\cdot H_2O$ (**2**) is coordinated by five S atoms and one N atom of the SCN^- ligands with a C_{4v} symmetry. Structural trans influence observed in the bond length of Rh−S at the trans position of Rh−N is 2.3398(13) Å, significantly shorter than those of **1** by ca. 0.04 Å, although DFT calculations based on the crystal structures indicated that the effective bond order of Rh−N is higher than those of Rh−S. Thermal stability examination by thermogravimetric and differential thermal analyses (TG/DTA) and IR spectroscopy indicated that the linkage isomerization of $[Rh^{III}(NCS)(SCN)_5]^{3-}$ proceeded after melting around 174 °C. These results clearly indicate that $[Rh^{III}(NCS)(SCN)_5]^{3-}$ is thermodynamically more stable than $[Rh^{III}(SCN)_6]^{3-}$ in solid states, although further linkage isomerization hardly occurs.

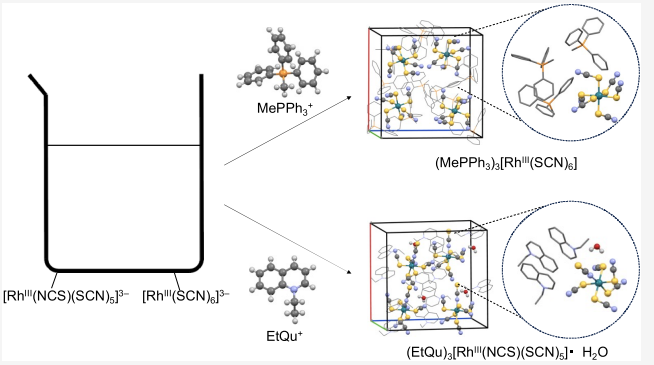

INTRODUCTION

Mononuclear metal complexes with multiple bridging ligands are potential candidates for critical building units of functional coordination polymers.[1−3] Among the bridging ligands, ambidentate ligands, which are bidentate but not chelate ligands, attract much attention because they enable the alignment of different metal ions alternatively.[4−6] Thiocyanate (SCN^-) is the most useful ambidentate ligand that can coordinate to a metal ion by an S and/or N atom.[7−11] S and N atoms of the SCN^- ligand are expected to coordinate to soft and hard metal ions, respectively.[12] In fact, the first raw transition metal ions, Cr^{III},[13] Mn^{II},[14] Fe^{III},[15] and Co^{III},[16] classified as hard Lewis acid, tend to form N-bound complexes, so-called isothiocyanate complexes, $[M(NCS)_6]^{n-}$. Also, metal ions such as Pd^{II},[17] Pt^{II},[18] and Au^{III}[19] ions, classified as soft Lewis acid, are coordinated by soft S atoms to form thiocyanate complexes, $[M(SCN)_4]^{n-}$. On the other hand, the formation of various linkage isomers has been reported for borderline Lewis acids including Ru^{III},[20] Os^{III},[21] Rh^{III},[22] and Ir^{III}.[23] These coordination isomers of $[M^{III}(NCS)_n(SCN)_{6-n}]^{3-}$ (n = 1−5 for M = Ru;[20] n = 0−6 for Os;[21] n = 0−4 for Rh;[22] n = 0−5 for Ir[23]) were separately isolated by column chromatography. The isolated coordination isomers were well-characterized by several spectroscopic techniques including IR, Raman, and NMR.[20−24] However, very limited information on X-ray crystal structures of linkage isomers is currently available, although structural information including structural trans influence is important to discuss the difference in various chemical properties of each linkage isomer including isomerization behaviors.[25]

Single-crystal X−ray structure analyses of (isothiocyanato)-(thiocyanato) complexes have been reported for $[Re^{IV}(NCS)_5(SCN)]^{2-}$ and $[Ir^{III}(NCS)(SCN)_5]^{3-}$ together with the corresponding hexa(thiocyanato) complexes.[26,27] Obvious structural trans influence was observed for the Re^{IV} (d^3) complex of $[Re^{IV}(NCS)_5(SCN)]^{2-}$, in which the bond length of Re−N at the trans position of Re−S was significantly longer than those at the cis positions.[26] On the other hand, no obvious structural trans influence was reported for the complexes containing d^6 metal ions, Ir^{III} and Co^{III}.[27,28] The single crystal of $(n\text{-}Bu_4N)_3[Ir^{III}(NCS)(SCN)_5]$ involves two

Received: July 6, 2023

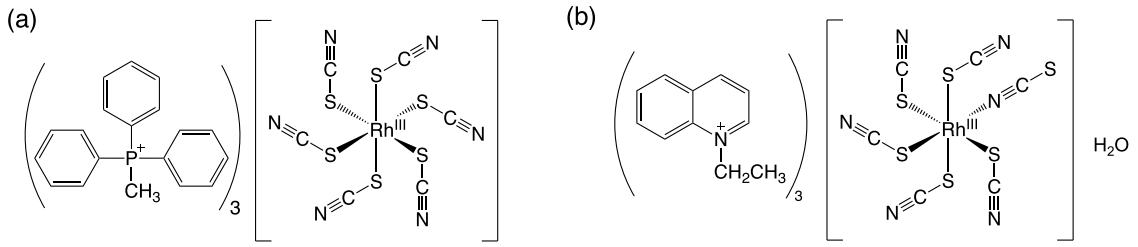

Figure 1. Chemical structures of (a) $(MePPh_3)_3[Rh^{III}(SCN)_6]$ (**1**) and (b) $(EtQu)_3[Rh^{III}(NCS)(SCN)_5]\cdot H_2O$ (**2**).

crystallographically independent $[Ir^{III}(NCS)(SCN)_5]^{3-}$ moieties in a unit cell.[27] One $[Ir^{III}(NCS)(SCN)_5]^{3-}$ moiety clearly shows the structural trans influence where the Ir−S bond length at the trans position of the Ir−N is slightly shorter than those at cis positions; however, the other $[Ir^{III}(NCS)(SCN)_5]^{3-}$ moiety has longer Ir−S at the trans position of Ir−N.[27] Similarly, no structural trans influence was observed for the single crystals of Co^{III} complexes, $[Co^{III}(SCN)(NH_3)_5]Cl_2$ and $[Co^{III}(NCS)(NH_3)_5]Cl_2$, both of which possess virtually the same Co−N(H_3) bond lengths at the trans positions of Co−SCN and Co−NCS.[28] However, the structural trans influence of the N- or S-bound SCN^- ligand for the Rh^{III} (d^6) complex has yet to be clarified for homoleptic (iso)thiocyanate complexes.

The complexes with d^6 metal ions usually tend to form thermodynamically stable octahedral complexes because of the maximum ligand field stabilization energy at the low spin state. We report herein the single-crystal X-ray structures of linkage isomers of thiocyanato mononuclear Rh(III) complexes, $[Rh^{III}(SCN)_6]^{3-}$ and $[Rh^{III}(NCS)(SCN)_5]^{3-}$, with counter-cations chosen from methyltriphenylphosphonium ($MePPh_3^+$) and 1-ethylquinolinium ($EtQu^+$), respectively. IR and Raman spectral measurements were performed for $(MePPh_3)_3[Rh^{III}(SCN)_6]$ (**1**) and $(EtQu)_3[Rh^{III}(NCS)(SCN)_5]\cdot H_2O$ (**2**) together with theoretical DFT calculations to discuss the bond characters of Rh−S and Rh−N (Figure 1). Additionally, the thermal stability and electrochemical properties of $[Rh^{III}(SCN)_6]^{3-}$ and $[Rh^{III}(NCS)(SCN)_5]^{3-}$ were investigated by thermogravimetric and differential thermal analyses (TG/DTA) and IR spectroscopy. The SCN^- ligand can be a crucial component of coordination polymers (CPs) including metal−organic frameworks.[29−35] The information on structural trans influence and thermal stability in monomeric complexes with the SCN^- ligand benefits the rational design of topologies of CPs with high thermal stability.

EXPERIMENTAL SECTION

Materials. All chemicals were used as supplied without further purification. Potassium thiocyanate, rhodium(III) chloride trihydrate, methyltriphenylphosphonium chloride ($MePPh_3Cl$), acetonitrile, and absolute ethanol were purchased from FUJIFILM-Wako Pure Chemical Industries Corporation. 1-Ethylquinolinium iodide (EtQuI) was obtained from Tokyo Chemical Industry Co., Ltd. Aqueous solutions were prepared with ultrapure water provided by a Barnstead Smart2Pure water purification system (Thermo Scientific) where the electronic conductance was 18.2 MΩ cm.

Preparation of the Stock Solution of $K_3[Rh^{III}(SCN)_6]$. The stock solution of $K_3[Rh^{III}(SCN)_6]$ was prepared according to the literature procedure with some modifications.[31] An aqueous solution of potassium thiocyanate (1.0 M, 30 mL) was heated to 100 °C and magnetically stirred, followed by the slow addition of an aqueous solution of rhodium(III) chloride trihydrate (0.57 M, 10 mL) for 2 h. After the reaction solution was cooled to room temperature, distilled water (25 mL) was slowly added to the obtained slurry and then evaporated under reduced pressure. After this procedure was repeated two times, absolute ethanol was added to the residue to extract the crude products. The insoluble residue was removed by filtration and the filtrate was evaporated to dryness under reduced pressure to obtain $K[Rh^{III}(SCN)_4]$. The formation of $K[Rh^{III}(SCN)_4]$ was confirmed by a characteristic CN stretching band appearing at 2109 cm^{-1} in the IR spectrum (Figure S1).[31] Then, $K[Rh^{III}(SCN)_4]$ thus obtained was dissolved in an aqueous solution containing KSCN (1.5 M, 105 mL) with stirring for 6 h at 60 °C. The obtained aqueous solution was used as the stock solution of $K_3[Rh^{III}(SCN)_6]$ (54 mM).

*Synthesis of $(MePPh_3)_3[Rh^{III}(SCN)_6]$ (**1**).* The stock solution of $K_3[Rh^{III}(SCN)_6]$ (54 mM, 10 mL) was added to an aqueous solution containing $MePPh_3Cl$ (1.0 M, 2.0 mL) with vigorous stirring at room temperature. The obtained orange crystalline powder was collected by centrifugation, washed with distilled water and acetone several times, and dried in vacuo at room temperature. Needle crystals of $(MePPh_3)_3[Rh^{III}(SCN)_6]$ suitable for single-crystal X-ray analysis were obtained by recrystallization from acetonitrile. Anal. Calcd for $C_{63}H_{54}N_6P_3RhS_6$: C, 58.96; H, 4.24; N, 6.55. Found C, 59.18; H, 4.34; N, 6.32. Yield: 520 mg (81%).

*Synthesis of $(EtQu)_3[Rh(NCS)(SCN)_5]\cdot H_2O$ (**2**).* The stock solution of $K_3[Rh^{III}(SCN)_6]$ (54 mM, 9.2 mL) was added to an aqueous solution containing EtQuI (1.0 M, 2.0 mL) with vigorous stirring at room temperature, resulting in orange supernatant with a small portion of reddish oil. Orange crystals suitable for single-crystal X-ray analysis formed in the supernatant separated from the oil after cooling at 4 °C for ∼3 months. Anal. Calcd for $C_{39}H_{38}N_9ORhS_6$: C, 49.61; H, 4.06; N, 13.36. Found C, 49.62; H, 3.99; N, 13.46. Yield: 72 mg (15%).

Single-Crystal X-ray Structural Analysis. Single-crystal X-ray structural analyses were carried out using a Rigaku AFC/Mercury CCD diffractometer with Mo Kα radiation (λ = 0.71073 Å) monochromated by graphite. The crystal structures were solved by a direct method using SIR92 and refined by the full-matrix least-squares method on F^2 with anisotropic displacement parameters for non-hydrogen atoms using SHELXL-2014.

DFT Calculations. All quantum chemical calculations were carried out with DFT calculation using the Gaussian 16W program package (Gaussian Inc.).[36] Calculations were conducted using the B3LYP/LANAL2DZ method.[37−39] Single-point calculations were performed only for the anions parts of **1** and **2** based on single-crystal X-ray structure analyses.

Physical Measurements. Infrared (IR) absorption spectra were obtained on a JASCO FT/IR-6700 spectrometer for the samples pelletized with potassium bromide (KBr). Raman spectra were taken on a JASCO NRS-4500 Raman spectrometer with a 532 nm excitation laser. Thermogravimetric and differential thermal analyses (TG/DTA) were carried out using a Rigaku Thermo plus EVO2 instrument equipped with an optical microscope. A weighed sample (∼5 mg) in a platinum pan was heated from room temperature to 500 °C in an Ar flow (50 mL min^{-1}) with a ramp rate of 5 or 1 °C min^{-1}.

RESULTS AND DISCUSSION

Synthesis and Isolation of $[Rh^{III}(SCN)_6]^{3-}$ and $[Rh^{III}(NCS)(SCN)_5]^{3-}$. The canonical structures of the

https://doi.org/10.1021/acs.inorgchem.3c02292
Inorg. Chem. XXXX, XXX, XXX−XXX

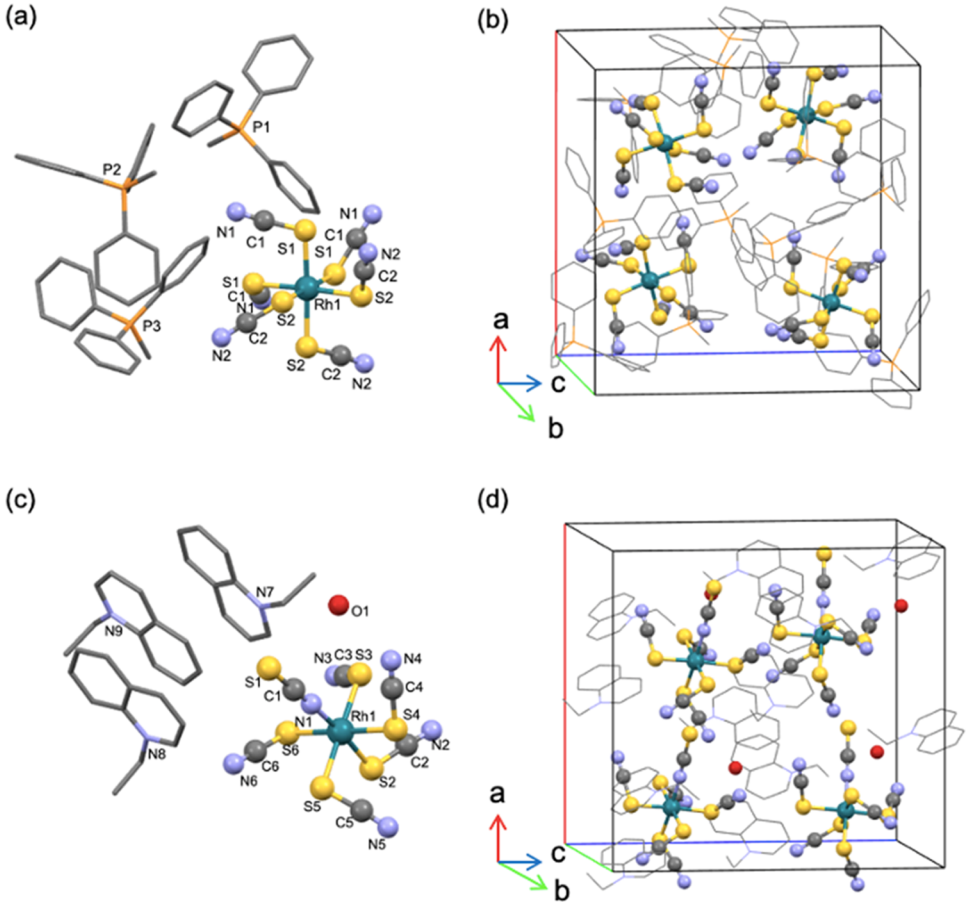

Figure 2. Crystal structures of crystallographically independent components and packing diagrams in unit cells. [(a, b) $(MePPh_3)_3[Rh^{III}(SCN)_6]$ (**1**) and (c, d) $(EtQu)_3[Rh^{III}(NCS)(SCN)_5]\cdot H_2O$ (**2**)]. Atoms are color coded as follows: Rh, green; C, gray; N, light blue; S, yellow; P, orange; and O, red. A unit cell is represented by a square. *a*-axis is a red line; *b*-axis is a green line; *c*-axis is a blue line.

ambidentate SCN^- ligand can be expressed as follows (eq 1).[40,41] Both S and N atoms are

$$[^-S{-}C{\equiv}N \leftrightarrow S{=}C{=}N^-] \quad (1)$$

negatively charged to readily coordinate with a metal ion. The hard−soft acid−base theory known as the HSAB theory predicts that the coordination of the softer S atom to the Rh^{III} ion seems to be more favorable than that of the harder N atom.[22] However, simple mixing of aqueous solutions of Rh^{III} ion and SCN^- ligand has been previously reported to provide a mixture of $[Rh^{III}(NCS)_n(SCN)_{6-n}]^{3-}$ (n = 0−1).[42] The isolated product yields of $[Rh^{III}(SCN)_6]^{3-}$ and $[Rh^{III}(NCS)(SCN)_5]^{3-}$ were 52 and 41%, respectively, with small amounts of other isomers in an aqueous solution at 60 °C, and negligible linkage isomerization proceeded under room temperature.[22] The linkage isomerization at elevated temperature has been also reported for $[Rh^{III}(NH_3)_5(SCN)]^{2+}$ and $[Rh^{III}(NH_3)_5(NCS)]^{2+}$, where the isomerization from $[Rh^{III}(NH_3)_5(SCN)]^{2+}$ to $[Rh^{III}(NH_3)_5(NCS)]^{2+}$ proceeded irreversibly by heating at 78 °C for 3 h, although no isomerization proceeded at 40 °C for 48 h.[42]

$[Rh^{III}(SCN)_6]^{3-}$ and $[Rh^{III}(NCS)(SCN)_5]^{3-}$ synthesized by the reaction of $[Rh^{III}(SCN)_4]^-$ with a large excess amount of KSCN were separated by crystallization with $MePPh_3^+$ or $EtQu^+$ ion. The addition of the reaction solution to an aqueous solution containing $MePPh_3^+$ immediately formed a crystalline powder. The obtained powder was collected by filtration and recrystallized as $(MePPh_3)_3[Rh^{III}(SCN)_6]$ (**1**) from MeCN in high yield (81%). Instead, the addition to an aqueous solution containing $EtQu^+$ ion provided an oily compound but no solid precipitate for a while. The crystals of $(EtQu)_3[Rh^{III}(NCS)(SCN)_5]\cdot H_2O$ (**2**) including one water molecule appeared in the separated supernatant after cooling at 4 °C for a couple of months with an isolation yield of 15%. The selective crystallization of **1** and **2** was evidenced by the powder X-ray diffraction patterns as shown in Figure S2. The patterns were virtually the same as those simulated from the single-crystal X-ray structure analysis of **1** and **2**. A reason for the selective crystallization can be ascribed to the symmetry of each countercation. $MePPh_3^+$ belongs to the C_{3v} point group with the symmetry element of the C3 axis, which is also included in the O_h point group of $[Rh^{III}(SCN)_6]^{3-}$ but not the C_{4v} point group of $[Rh^{III}(NCS)(SCN)_5]^{3-}$. Thus, crystals containing $MePPh_3^+$ and $[Rh^{III}(SCN)_6]^{3-}$, not $[Rh^{III}(NCS)(SCN)_5]^{3-}$, are selectively formed. On the other hand, the addition of nonsymmetric $EtQu^+$ to the reaction solution provided oily products as the first crop. Crystals of **2** are formed in the separated supernatant involving a crystallizing water molecule, which forms hydrogen bonds with N and S atoms of SCN^- ligands.

Crystal Structures of $(MePPh_3)_3[Rh^{III}(SCN)_6]$ (1) and $(EtQu)_3[Rh^{III}(NCS)(SCN)_5]\cdot H_2O$ (2). The crystal structures of $(MePPh_3)_3[Rh^{III}(SCN)_6]$ (**1**) and $(EtQu)_3[Rh^{III}(NCS)(SCN)_5]\cdot H_2O$ (**2**) were solved to determine the coordination modes of the six SCN^- ligands by single-crystal X-ray structure analyses (Figure 2). Crystallographic parameters and selected f2t1t2

https://doi.org/10.1021/acs.inorgchem.3c02292
Inorg. Chem. XXXX, XXX, XXX−XXX

atomic distances and angles are given in Tables 1 and 2, respectively. In a previous report, $[Rh^{III}(SCN)_6]^{3-}$ crystallized in the centric space group of *Cc* (monoclinic) using PPh_4^+ as the countercation.[43] On the other hand, **1** crystallized in the noncentric space group of $P2_13$ (cubic) in which the Rh^{III} ion has the octahedral geometry by the coordination of six S atoms from SCN^- ligands, in which only two of six SCN^- ligands are crystallographically independent. The highly symmetric structure resulted from the countercation with C3 symmetry, $MePPh_3^+$, where P atoms can also sit on the C3 axis as well as the Rh ion. The observed bond lengths of Rh−S (2.3675(14) and 2.3808(14) Å) and Rh−S−C angles (106.2(2) and 108.3(3)°) in **1** are within the typical range of those reported for $(PPh_4)_3[Rh^{III}(SCN)_6]$ (Rh−S: 2.348(5)−2.396(6) Å and Rh−S−C: 108.1(6)−110.5(7)°).[43]

Table 1. Crystallographic Parameters for $(MePPh_3)_3[Rh^{III}(SCN)_6]$ (1) and $(EtQu)_3[Rh^{III}(NCS)(SCN)_5]\cdot H_2O$ (2)

	$(MePPh_3)_3[Rh^{III}(SCN)_6]$	$(EtQu)_3[Rh^{III}(NCS)(SCN)_5]\cdot H_2O$
formula	$C_{63}H_{54}N_6P_3RhS_6$	$C_{39}H_{38}N_9ORhS_6$
formula Weight	1283.3	944.05
temperature, K	150(2)	110(2)
crystal system	Cubic	Monoclinic
space group	$P2_13$	*Cc*
Z	4	4
a, Å	18.0867(4)	17.9779(9)
b,Å	18.0867(4)	12.0511(7)
c, Å	18.0867(4)	18.9372(11)
α, deg	90	90
β, deg	90	91.065(3)
γ, deg	90	90
V, Å^3	5916.7(4)	4102.1(4)
density, g cm^{-3}	1.441	1.529
GOF	1.261	1.008
R_1 [$I > 2\sigma(I)$]	0.0499	0.0362
wR_2 for all data	0.1249	0.0747

Table 2. Selected Bond Lengths and Angles for $(MePPh_3)_3[Rh^{III}(SCN)_6]$ (1) and $(EtQu)_3[Rh^{III}(NCS)(SCN)_5]\cdot H_2O$ (2)

$(MePPh_3)_3[Rh^{III}(SCN)_6]$ (**1**)		$(EtQu)_3[Rh^{III}(NCS)(SCN)_5]\cdot H_2O$ (**2**)	
atoms	length, Å	atoms	length, Å
Rh1−S1	2.3675(14)	Rh1−N1	2.044(4)
Rh1−S2	2.3808(14)	Rh1−S2	2.3398(13)
		Rh1−S3	2.3807(13)
		Rh1−S4	2.3756(15)
		Rh1−S5	2.3832(14)
		Rh1−S6	2.3828(14)
S1−C1	1.679(6)	S1−C1	1.639(5)
S2−C2	1.650(7)	S2−C2	1.657(5)
		S3−C3	1.678(6)
		S4−C4	1.670(6)
		S5−C5	1.667(6)
		S6−C6	1.686(6)
C1−N1	1.157(8)	C1−N1	1.150(7)
C2−N2	1.171(9)	C2−N2	1.160(7)
		C3−N3	1.162(7)
		C4−N4	1.140(8)
		C5−N5	1.150(7)
		C6−N6	1.151(7)
atoms	angle, deg	atoms	angle, deg
Rh1−S1−C1	106.2(2)	Rh1−N1−C1	177.3(4)
Rh1−S2−C2	108.3(2)	Rh1−S2−C2	109.17(18)
		Rh1−S3−C3	105.19(17)
		Rh1−S4−C4	102.42(19)
		Rh1−S5−C5	103.84(19)
		Rh1−S6−C6	102.55(19)

2 crystallized in the space group of *Cc* (monoclinic) with a $[Rh^{III}(NCS)(SCN)_5]^{3-}$, three $EtQu^+$, and one water as crystallographically independent molecules (Figure 2c). The positions of H atoms of the crystallizing water molecule were determined based on the electron density map. The hydrogen atoms of the water molecule are directed to N4 and S1 of SCN^- ligands in the suitable distances for hydrogen bond formation. **2** also has an octahedral geometry around the Rh^{III} ion but is coordinated by five S atoms and one N atom of SCN^- ligands with the C_{4v} symmetry. Four Rh−S bond lengths at the cis positions of the Rh−N were 2.3756(15)−2.3828(14) Å similar to those in **1**; however, the Rh−S bond length at the trans position of Rh−N was significantly shorter as 2.3398(13) Å by ca. 0.04 Å corresponding to 1.7% of average Rh−S bond length of **1**. The shorter Rh−S bond resulted from the weak structural trans influence of the N-bound SCN^- ligand compared with the S-bound SCN^- ligand in the mononuclear Rh^{III} complexes.

The Rh−S−C angle of **2** was slightly wider at the trans position of Rh−N, 109.17(18)° compared with those at cis positions, 102.42(19)−105.19(17)°, suggesting that the p-character of the sp^3 hybrid orbital of the sulfur slightly diminished due to p*π*−d*π* interaction between S and Rh ion at the trans position of Rh−N. In general, the S-bound SCN^- ligand can act as both *σ*-donor and *π*-donor; on the other hand, the N-bound SCN^- ligand as a *σ*-donor and a *π*-acceptor.[25,44] The Rh^{III} ion of **1** has six d-electrons, fully occupying the t_{2g} orbitals with the low spin state, suggesting that the *π*-donor property of the S-bound SCN^- ligand can be ignored. However, the coordination of N to the Rh^{III} ion in **2** reduced the electron density of the d-orbital by *π*-back-donation, resulting in the S-bound SCN^- ligand being able to act as a *π*-donor only at the trans position of Rh−N.

The structures of SCN^- ligands were then carefully examined because the coordination isomers were often discriminated by vibrational spectra including IR and Raman spectra (vide infra). The S−C bond lengths of the S-bound SCN^- ligands are between 1.657(6) and 1.678(6) Å, which are longer than that of the N-bound SCN^- ligand, 1.638(6) Å. On the other hand, no obvious difference was observed in the C−N bond lengths between 1.141(8) and 1.162(7) Å for all of the SCN^- ligands. Thus, the N-bound SCN^- ligand has a shorter S−C bond length; however, the difference in the C−N bond lengths compared with the S-bound SCN^- ligands was insignificant. The N-bound SCN^- ligand forms a hydrogen bond with the crystallizing water molecule; however, its effect on S−C bond length can be ignored because the hydrogen bond formation usually elongates chemical bonds with bonding character.

The structural trans influence of the S-bound SCN^- ligand in a homoleptic Re^{IV} (d^3) complex can be evaluated from the crystal-structure comparison of $[Re^{IV}(NCS)_5(SCN)]^{2-}$ with $[Re^{IV}(NCS)_6]^{2-}$.[26] The bond length of Re−N at the trans position of Re−S was 2.150(5) Å, which is longer than the

https://doi.org/10.1021/acs.inorgchem.3c02292
Inorg. Chem. XXXX, XXX, XXX−XXX

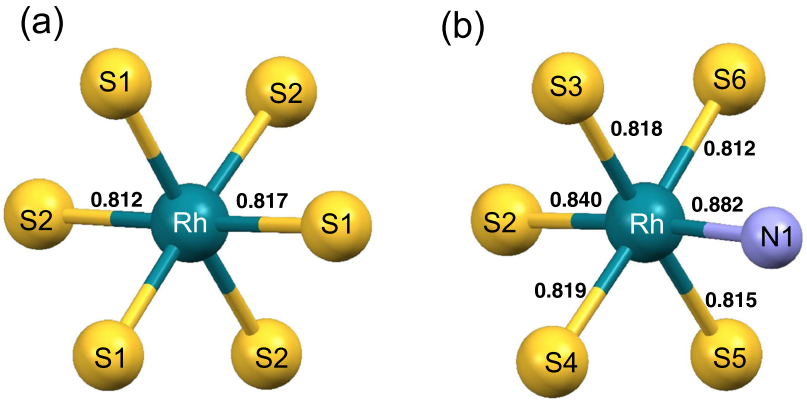

Figure 3. Effective bond orders of Rh−S and Rh−N in (a) $[Rh^{III}(SCN)_6]^{3-}$ and (b) $[Rh^{III}(NCS)(SCN)_5]^{3-}$ estimated by DFT calculations.

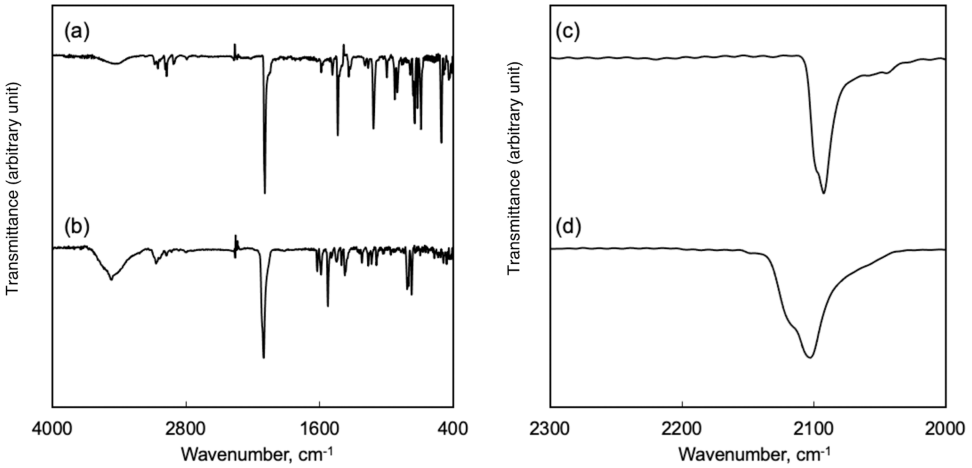

Figure 4. IR spectra of (a, c) $(MePPh_3)_3[Rh^{III}(SCN)_6]$ (**1**) and (b, d) $(EtQu)_3[Rh^{III}(NCS)(SCN)_5]\cdot H_2O$ (**2**) in KBr pellets. (a, b) Wide range and (c, d) CN stretching region (2000−2300 cm^{-1}).

average Re−N length reported for $[Re^{IV}(NCS)_6]^{2-}$, 2.045 Å, by 0.11 Å (5.1%), indicating that the strong electron-donating ability of the S-bound SCN^- ligand plays a crucial role in the structural trans influence. Also, the structural cis influence observed in $[Re^{IV}(NCS)_5(SCN)]^{2-}$ evidenced the strong electron-donating ability of the S-bound SCN^- ligand, where the average Re−N bond length of 2.009 Å in $[Re^{IV}(NCS)_5(SCN)]^{2-}$ is shorter than those of 2.045 Å in $[Re^{IV}(NCS)_6]^{2-}$ by 0.036 Å (1.8%).[26]

The structural trans influence observed in the Rh^{III} (d^6) complexes seems weaker when compared with that in the Re^{IV} (d^3) complexes; however, it is more obvious compared with those in the complexes containing the same d^6 metal ions including Ir^{III} and Co^{III}. The structural trans influence in Ir^{III} complexes can be examined by the crystal structure of $(n\text{-}Bu_4N)_3[Ir^{III}(NCS)(SCN)_5]$.[27] The complex crystallized in the space group of $P2_1/a$ including two crystallographically independent $[Ir^{III}(NCS)(SCN)_5]^{3-}$ complexes.[27] The first $[Ir^{III}(NCS)(SCN)_5]^{3-}$ has a significantly shorter Ir−S bond at the trans position of Ir−N, 2.327(3) Å compared with the Ir^{III}−S bond lengths at the cis positions, 2.356(4)−2.383(3) Å.[27] However, the second $[Ir^{III}(NCS)(SCN)_5]^{3-}$ has the Ir−S bond length of 2.384(4) Å at the trans position of Ir−N, which is somewhat longer than those at the cis positions, 2.294(4)−2.373(4) Å.[27] In the case of Co^{III}, no crystallographic structure is available for homoleptic compounds using the SCN^- ligand; however, single-crystal structures of thiocyanate and isothiocyanate pentaammine complexes, i.e., $[Co^{III}(SCN)(NH_3)_5]Cl_2$ and $[Co^{III}(NCS)(NH_3)_5]Cl_2$, have been reported to clarify the structural trans influence.[28] The Co−N bond lengths in $[Co^{III}(SCN)(NH_3)_5]Cl_2$ were almost the same at the trans and cis positions of the S-bound SCN^- ligands, 1.93(2) and 1.93(2)−1.96(2) Å, respectively.[28] In $[Co^{III}(NCS)(NH_3)_5]Cl_2$, the Co−N bond length at the trans position of Co−N(CS) was 1.90(2) Å, which was virtually the same as those at the cis positions, 1.90(2) Å.[28] Further, the structural information about various isomers of the Rh^{III} complexes is necessary to elucidate a reason for the obvious structural trans influence of the SCN^- ligand in Rh^{III} complexes.

DFT Calculations. The structural trans influence was confirmed by theoretical calculations for single-point DFT calculations of $[Rh^{III}(SCN)_6]^{3-}$ and $[Rh^{III}(NCS)(SCN)_5]^{3-}$ based on the anion parts of crystal structures of **1** and **2**. The average effective bond order around Rh−S in **1** was 0.815 as calculated from the natural orbital occupation numbers divided by 2 (Figure 3a). The effective bond order of Rh−S at the trans position of Rh−N in **2** was 0.840, which is much higher than that of four Rh−S bonds of **2** at the cis positions, 0.812−0.819 (average 0.815, Figure 3b). The higher effective bond order of Rh−S at the trans position resulted from the less negative charge of the N atom than that of the S atom of the SCN^- ligand, which is −0.219 and −0.364, respectively, as indicated by the Mulliken charges obtained by DFT calculations (Figure S3a). The effective bond order of Rh−N

https://doi.org/10.1021/acs.inorgchem.3c02292
Inorg. Chem. XXXX, XXX, XXX−XXX

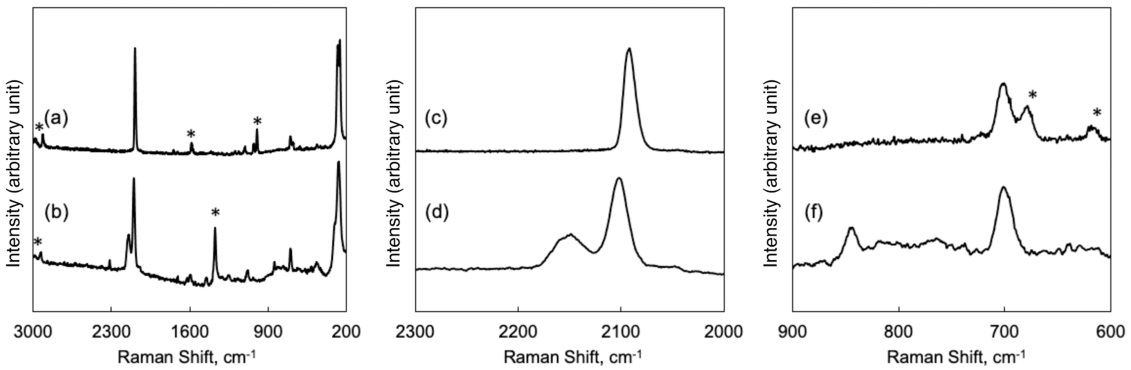

Figure 5. Raman spectra of (a, c, e) $(MePPh_3)_3[Rh^{III}(SCN)_6]$ (**1**) and (b, d, f) $(EtQu)_3[Rh^{III}(NCS)(SCN)_5]\cdot H_2O$ (**2**). (a, b) Wide range, (c, d) CN stretching region, and (e, f) CS stretching region. Excited light: λ = 532.5 nm. The peaks with * originated from countercations.

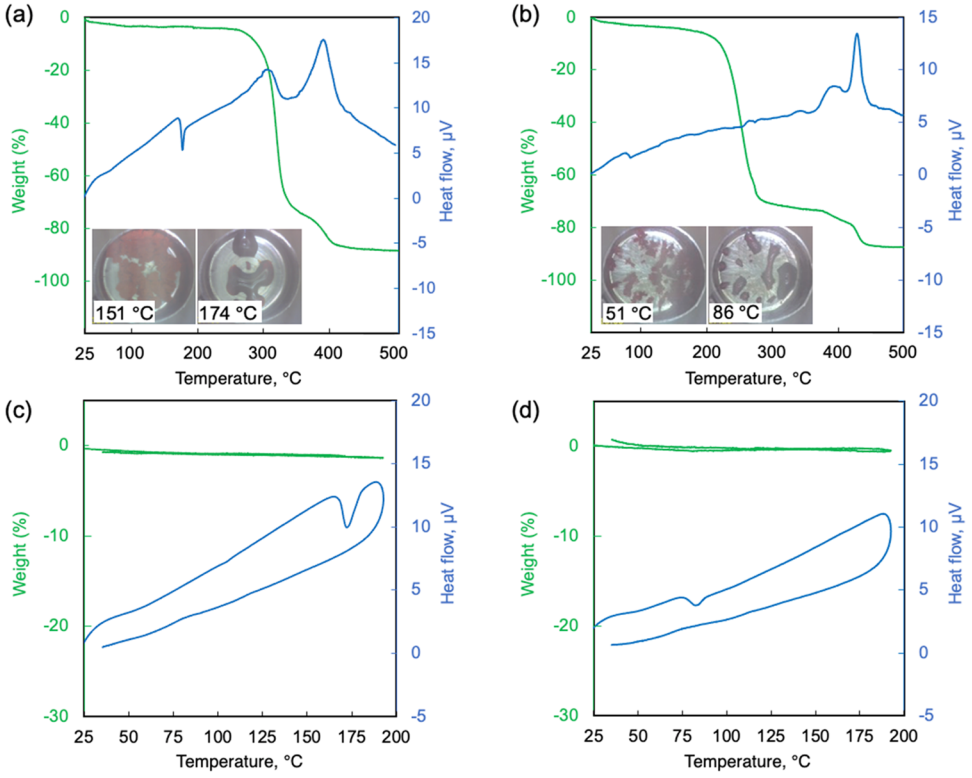

Figure 6. Thermogravimetric analyses (TGA, green lines) and differential thermal analyses (DTA, blue lines) of (a) $(MePPh_3)_3[Rh^{III}(SCN)_6]$ (**1**) heated to 500 °C, (b) $(EtQu)_3[Rh^{III}(NCS)(SCN)_5]$ (**2**) heated to 500 °C, (c) **1** heated to 185 °C and cooled to room temperature, and (d) **2** heated to 185 °C and cooled to room temperature in an Ar flow. The insets in parts (a) and (b) are photographs of each sample in solid and melting states.

was 0.882 higher than that of Rh−S resulting from the π-acceptor character of the N atom of the SCN^- ligand. Although these results clearly indicate that the formation of the *trans*(isothiocyanato)(thiocyanato) rhodate(III) structure (SCN−Rh−SCN) is thermodynamically more stable than the *trans*(thiocyanato)(thiocyanato) structure (NCS−Rh−SCN), only two isomers of $[Rh^{III}(NCS)_n(SCN)_{6-n}]^{3-}$ (n = 0 or 1) predominantly formed in solution.[22] Further isomerization to $[Rh^{III}(NCS)_n(SCN)_{6-n}]^{3-}$ ($n \geq 2$) is possible as reported previously but proceeds less favorably[22] because the Rh^{III} ion coordinated by the N atom of SCN^- ligand becomes a softer Lewis acid than that coordinated by the S atom, resulting from the delocalization of d-electrons of the Rh^{III} ion to the N-bound SCN^- ligand due to its stronger π-acceptor property.

IR and Raman Spectra of $(MePPh_3)_3[Rh^{III}(SCN)_6]$ (1) and $(EtQu)_3[Rh^{III}(NCS)(SCN)_5]\cdot H_2O$ (2). **1** and **2** have been scrutinized by IR and Raman spectral measurements as shown in Figures 4 and 5. The IR spectra were taken by the KBr pellet method after confirming that no ligand exchange occurred from SCN^- to Br^- by using the ATR method (Figure S4). The CN stretching band (ν(CN)) of **1** appeared at 2092 cm^{-1} accompanied by a shoulder peak around 2098 cm^{-1} in the IR spectrum (Figure 4a,c). Such double peaks often reported for thiocyanato and isothiocyanato complexes seem to reflect a subtle difference in coordination structures, evidenced by the single peak in the IR spectrum in solution (Figure S7). However, the Raman spectrum of **1** in the solid state showed no shoulder peak in the ν(CN) region as shown in Figure 5a,c,[4b] indicating that the sensitivity to a trivial

https://doi.org/10.1021/acs.inorgchem.3c02292
Inorg. Chem. XXXX, XXX, XXX−XXX

difference in crystal structures depends on each spectroscopy. The peak positions of ν (CN) and ν(CS) bands appearing at 2091 and 700 cm^{-1}, respectively, in the Raman spectra shown in Figure 5c,e were virtually the same as those reported for (n-$Bu_4N)_3[Rh^{III}(SCN)_6]$ appearing at 2098 and 700 cm^{-1}, respectively.[22]

The ν (CN) bands of **2** appeared at 2102 cm^{-1} accompanied by the shoulder peak around 2115 cm^{-1} in the IR spectrum (Figure 4b). The Raman spectrum of **2** showed two more clearly separated peaks at 2100 and 2146 cm^{-1} in the ν(CN) region (Figure 5d). The shoulder peak at higher wavenumber can be assigned to ν(CN) of the N-bound SCN^- ligand, which is similar to the difference in ν(CN) of $[Rh^{III}(NH_3)_5(SCN)]^{2+}$ and $[Rh^{III}(NH_3)_5(NCS)]^{2+}$, 2115 and 2145 cm^{-1}, respectively.[42] The difference in the ν(CN) bands observed in IR and Raman spectra was also reported previously for μ(N,S)-thiocyanato-μ(N,O,O,O′-picolinato)cadmium(II), in which singlet ν(CN) band appeared at 2080 cm^{-1} in the IR spectrum; however, two peaks at 2125 and 2085 cm^{-1} appeared in the Raman spectrum.[45] Vibrational spectrum analysis based on the DFT calculation was performed for $[Rh^{III}(NCS)(SCN)_5]^{3-}$ with the crystallizing water molecule; however, all of the ν(CN) bands are active for both IR and Raman spectroscopies (Figure S5). Thus, the crystal packing may have an effect on the peak positions of ν(CN) bands in the IR spectrum. In the C−S stretching band region, two ν(CS) peaks appeared at 699 and 845 cm^{-1} in the Raman spectrum of **2** (Figure 5f). The ν(CS) peak of the N-bound SCN^- ligand has been reported to appear around 835 cm^{-1} in the Raman spectra of $(n\text{-}Bu_4N)_3[Rh^{III}(NCS)_n(SCN)_{6-n}]$ ($n \geq 3$), although the peak was not clearly observed for $(n\text{-}Bu_4N)_3[Rh^{III}(NCS)(SCN)_5]$.[22] The peak appearing at 845 cm^{-1} in the Raman spectrum of **2** can be assigned to ν(CS) of the N-bound SCN^- ligand.

TG/DTA of $(MePPh_3)_3[Rh^{III}(SCN)_6]$ (1) and $(EtQu)_3[Rh^{III}(NCS)(SCN)_5]\cdot H_2O$ (2). Thermal behaviors of 1 and 2 were investigated by TG/DTA equipped with an optical microscope (Figure 6). TG analysis of **1** indicated that large weight loss (~65%) observed around 320 °C corresponds to the thermal decomposition of countercations, $MePPh_3^+$, with a slightly exothermic DTA peak, where the expected weight loss was 65% from the chemical formula. The successive weight loss up to 450 °C by 21% with the significant exothermic DTA peak was assigned to the thermal decomposition of SCN^- ligands, although the weight loss was smaller than expected from the chemical formula, 27%. The weight loss less than expected could result from the formation of Rh_2S_3 as the thermal decomposition residue where the expected remained weight of 12% of the total weight is close to the observed that of 11%.[46] Other than the two exothermic peaks, an endothermic peak appeared around 170 °C without weight loss (Figure 6a). The melting behavior of **1** was confirmed by the optical microscope as shown in Figure 6a (inset). No obvious weight loss during the melting process was further confirmed by slow heating of 1 °C min^{-1} from room temperature to 185 °C, followed by slow cooling to room temperature (Figure 6c). Similarly, TG analysis of **2** demonstrated that large weight loss (>70%) was observed around 230 °C, resulting from the thermal decomposition of $EtQu^+$ cations and desorption of crystallizing water molecule, which occupy 1.9% of total weight, without exo- or endothermic peak, where the expected weight loss was 53% from the chemical formula of **2**. The remained weight of 13% after heating at 500 °C corresponded to the formation of Rh_2S_3 where the expected remained weight is 11% of the total weight of **2**. The thermal decomposition of SCN^- ligands gradually proceeded from 250 to 420 °C. The DTA curve of **2** showed the endothermic peak around 85 °C with melting behavior (Figure 6b (inset) and 6d), which is ~90 °C lower than the melting point of **1**.

Thermal impact on the linkage isomerization of **1** and **2** after heating at higher than melting points was confirmed by the ν(CN) bands in IR spectra. The IR spectrum measured for **1** after melting at 185 °C exhibited a new shoulder peak at 2113 cm^{-1} due to ligand isomerization (Figure 7).

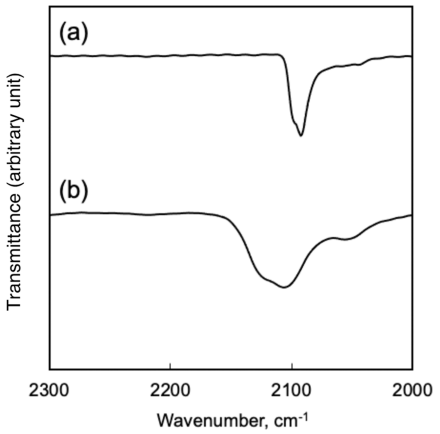

Figure 7. IR spectra of $(MePPh_3)_3[Rh^{III}(SCN)_6]$ (**1**) (a) before and (b) after heating at 185 °C.

Thus, the heating at a temperature higher than the melting point of **1** induced ligand isomerization from $[Rh^{III}(SCN)_6]^{3-}$ to $[Rh^{III}(NCS)(SCN)_5]^{3-}$. On the other hand, the IR spectrum of **2** after heating at 100 °C higher than the melting point exhibited ν(CN) peak shapes similar to that measured for **2** without heating, indicating no structural change in $[Rh^{III}(NCS)(SCN)_5]^{3-}$ (Figure S6a,b). No obvious change in the IR spectrum of **2** was also confirmed even after heating at 185 °C (Figure S6c). Thus, **2** is thermodynamically more stable than **1** in the solid state, as similarly observed in the solution state. The lower melting point of **2** is related to the countercation or the presence of crystallizing water, not to coordination modes of SCN^- ligands around the Rh(III) ion.

Electrochemical Behaviors of $(MePPh_3)_3[Rh^{III}(SCN)_6]$ and $(EtQu)_3[Rh^{III}(NCS)(SCN)_5]$. Cyclic voltammograms of **1** and **2** were recorded in acetonitrile. No coordination isomerization in the MeCN solution was confirmed by IR measurements (Figure S7). The peak positions of the ν(CN) peaks of **1** and **2** observed in MeCN solutions were virtually the same as those in the solid states. CV measurements for **1** and **2** were carried out at the potential ranging from −0.6 to 0.8 V vs Ag/Ag^+ with the scanning rate of 100 mV s^{-1} (Figure S8). Quasi-reversible redox couple assignable to $SCN^-/SCN^\bullet$ were obtained for both **1** and **2** with i_{pa}/i_{pc} = 0.70 and 0.91, respectively. The redox reversibility of KSCN was as low as i_{pa}/i_{pc} = 0.21 in MeCN because oxidized SCN^- ($SCN^\bullet$) has been reported to be partially dimerized to form $(SCN)_2$.[47] Thus, the high reversibility observed for **1** and **2** indicates that the coordination of SCN^- to Rh(III) ion suppresses the dimerization of oxidized SCN^- more effectively in **2**.

https://doi.org/10.1021/acs.inorgchem.3c02292
Inorg. Chem. XXXX, XXX, XXX−XXX

A reason for the high reversibility of **2** was scrutinized by DFT calculations. The DFT calculations suggested that the sextuply degenerate HOMOs (highest occupied molecular orbitals) of **1** located on the six sulfur atoms of SCN^- ligands, which directly coordinated to the Rh^{III} ion (Figures S9−S11). On the other hand, the doubly degenerate HOMOs of **2** are solely located on the S atom of the N-bound SCN^- ligand, indicating that the one-electron oxidation of **2** hardly influences the Rh−N bond strength, although that of **1** slightly affects the Rh−S bond strength (Figures S9−S12).

CONCLUSIONS

Linkage isomers of $[Rh^{III}(SCN)_6]^{3-}$ and $[Rh^{III}(NCS)(SCN)_5]^{3-}$ formed in the reaction solution were separately crystallized by using $MePPh_3^+$ and $EtQu^+$ as countercations. Comparison of the single-crystal structures of $(MePPh_3)_3[Rh^{III}(SCN)_6]$ (**1**) and $(EtQu)_3[Rh^{III}(NCS)(SCN)_5]\cdot H_2O$ (**2**) clearly indicated that the Rh−S bond is shorter at the trans position of Rh−N than that of Rh−S by ∼0.04 Å (1.7%). Thus, the structural trans influence of the N-bound SCN^- ligand is weaker than that of the S-bound one. The thermal stability of **1** and **2** examined by TG/DTA and IR measurements manifested that **2** is thermodynamically stable compared with **1**. Furthermore, the electrochemical measurements clarified that a one-electron oxidation−reduction process between −0.6 and 0.8 V vs Ag/Ag^+ assignable to $SCN^-/SCN^•$ is more reversible in **2** than in **1**, indicating that **2** is more tolerant to oxidation stress than **1**. The information is beneficial for designing polynuclear metal complexes, such as coordination polymers using SCN^- as a bridging ligand, with high stability under harsh conditions.

ASSOCIATED CONTENT

Supporting Information

The Supporting Information is available free of charge at https://pubs.acs.org/doi/10.1021/acs.inorgchem.3c02292.

IR spectra (Figures S1, S4, S6, and S7), XRD (Figure S2), CV (Figure S8), DFT calculation results (Mulliken charge of SCN^- ligand), orbitals and energy levels, vibrational spectra (Figures S3, S5, S9−S12) (PDF)

Accession Codes

CCDC 2277076−2277077 contain the supplementary crystallographic data for this paper. These data can be obtained free of charge via www.ccdc.cam.ac.uk/data_request/cif, or by emailing data_request@ccdc.cam.ac.uk, or by contacting The Cambridge Crystallographic Data Centre, 12 Union Road, Cambridge CB2 1EZ, U.K.; fax: +44 1223 336033.

AUTHOR INFORMATION

Corresponding Author

Yusuke Yamada − *Department of Chemistry and Bioengineering, Graduate School of Engineering, Osaka Metropolitan University, Sumiyoshi, Osaka 558-8585, Japan; Research Center for Artificial Photosynthesis (ReCAP), Osaka Metropolitan University, Sumiyoshi, Osaka 558-8585, Japan;* orcid.org/0000-0001-6259-5255; Email: ymd@omu.ac.jp

Authors

Miki Mukai − *Department of Chemistry and Bioengineering, Graduate School of Engineering, Osaka Metropolitan University, Sumiyoshi, Osaka 558-8585, Japan*

Seiya Hagiwara − *Department of Chemistry and Bioengineering, Graduate School of Engineering, Osaka Metropolitan University, Sumiyoshi, Osaka 558-8585, Japan*

Rika Tanaka − *Department of Chemistry and Bioengineering, Graduate School of Engineering, Osaka Metropolitan University, Sumiyoshi, Osaka 558-8585, Japan; Analytical Center of Osaka Metropolitan University, Sumiyoshi, Osaka 558-8585, Japan*

Hiroyasu Tabe − *Research Center for Artificial Photosynthesis (ReCAP), Osaka Metropolitan University, Sumiyoshi, Osaka 558-8585, Japan;* orcid.org/0000-0003-2028-7371

Takashi Nakazono − *Research Center for Artificial Photosynthesis (ReCAP), Osaka Metropolitan University, Sumiyoshi, Osaka 558-8585, Japan;* orcid.org/0000-0001-6244-6399

Complete contact information is available at: https://pubs.acs.org/10.1021/acs.inorgchem.3c02292

Author Contributions

The manuscript was written through contributions of all authors. All authors have given approval to the final version of the manuscript.

Funding

This work was supported by JSPS KAKENHI to Y.Y. (Nos. JP19KK0144; JP22H01871), H.T. (Nos. JP19K15591 and JP21K14648), and T.N. (Nos. JP20K15303 and JP23K04770) and the Joint Usage/Research Center for Catalysis (23AY0194).

Notes

The authors declare no competing financial interest.

REFERENCES

(1) Song, X.; Wang, Y.; Wang, C.; Wang, D.; Zhuang, G.; Kirlikovali, K. O.; Li, P.; Farha, O. K. Design Rules of Hydrogen-Bonded Organic Frameworks with High Chemical and Thermal Stabilities. *J. Am. Chem. Soc.* **2022**, *144* (24), 10663−10687.

(2) Lv, X. L.; Yuan, S.; Xie, L. H.; Darke, H. F.; Chen, Y.; He, T.; Dong, C.; Wang, B.; Zhang, Y. Z.; Li, J. R.; Zhou, H. C. Ligand Rigidification for Enhancing the Stability of Metal-Organic Frameworks. *J. Am. Chem. Soc.* **2019**, *141* (26), 10283−10293.

(3) Eddaoudi, M.; Sava, D. F.; Eubank, J. F.; Adil, K.; Guillerm, V. Zeolite-like metal-organic frameworks (ZMOFs): design, synthesis, and properties. *Chem. Soc. Rev.* **2015**, *44* (1), 228−249.

(4) (a) Burmeister, J. Ambidentate ligands, the schizophrenics of coordination chemistry. *Coord. Chem. Rev.* **1990**, *105* (1), 77−133. (b) Bailey, R. A.; Kozak, S. L.; Michelsen, T. W.; Mills, W. N. Infrared spectra of complexes of the thiocyanate and related ions. *Coord. Chem. Rev.* **1971**, *6* (4), 407−445.

(5) Norbury, A. H.; Sinha, A. I. P. The co-ordination of ambidentate ligands. *Quart. Rev., Chem. Soc.* **1970**, *24* (1), No. 69.

(6) Scandola, F.; Argazzi, R.; Bignozzi, C. A.; Chiorboli, C.; Indelli, M. T.; Rampi, M. A. Electronic coupling between remote metal centers in cyanobridged polynuclear complexes. *Coord. Chem. Rev.* **1993**, *125* (1−2), 283−292.

(7) Bassey, E. N.; Paddison, J. A. M.; Keyzer, E. N.; Lee, J.; Manuel, P.; da Silva, I.; Dutton, S. E.; Grey, C. P.; Cliffe, M. J. Strengthening the Magnetic Interactions in Pseudobinary First-Row Transition Metal Thiocyanates, $M(NCS)_2$. *Inorg. Chem.* **2020**, *59* (16), 11627−11639.

(8) Cliffe, M. J.; Lee, J.; Paddison, J. A. M.; Schott, S.; Mukherjee, P.; Gaultois, M. W.; Manuel, P.; Sirringhaus, H.; Dutton, S. E.; Grey, C. P. Low-dimensional quantum magnetism in $Cu(NCS)_2$: A molecular framework material. *Phys. Rev. B* **2018**, *97* (14), No. 144421, DOI: 10.1103/PhysRevB.97.144421.

(9) Shurdha, E.; Moore, C. E.; Rheingold, A. L.; Lapidus, S. H.; Stephens, P. W.; Arif, A. M.; Miller, J. S. First row transition metal(II) thiocyanate complexes, and formation of 1-, 2-, and 3-dimensional extended network structures of $M(NCS)_2(solvent)_2$ (M = Cr, Mn, Co) composition. *Inorg. Chem.* **2013**, *52* (18), 10583−10594.
(10) Boeckmann, J.; Näther, C. Metamagnetism and long range ordering in μ-1,3 bridging transition metal thiocyanato coordination polymers. *Polyhedron* **2012**, *31* (1), 587−595.
(11) (a) Preetz, W.; Peters, G.; Bublitz, D. Preparation and Spectroscopic Investigations of Mixed Octahedral Complexes and Clusters. *Chem. Rev.* **1996**, *96* (3), 977−1025. (b) Schmidtke, H. H.; Garthoff, D. Darstellung und Charakterisierung einiger Thiocyanat- und Selenocyanat-Komplexe von Übergangsmetallen. *Helv. Chim. Acta* **1967**, *50* (6), 1631−1638. (c) Sabatini, A.; Bertini, I. Infrared Spectra between 100 and 2500 $Cm.^{-1}$ of Some Complex Metal Cyanates, Thiocyanates, and Selenocyanates. *Inorg. Chem.* **1965**, *4* (7), 959−961. (d) Forster, D.; Goodgame, D. M. L. Isothiocyanato Complexes of Nickel(II) and Copper(II). *Inorg. Chem.* **1965**, *4* (6), 823−829. (e) Clark, R. J.; Goodwin, A. D. J. Infrared and laser Raman spectra of metal hexaisothiocyanate ions. *Spectrochim. Acta, Part A* **1970**, *26* (2), 823−829.
(12) Savard, D.; Leznoff, D. B. Synthesis, structure and light scattering properties of tetraalkylammonium metal isothiocyanate salts. *Dalton Trans.* **2013**, *42* (42), 14982−14991.
(13) Larkworthy, L. F.; Leonard, G. A.; Povey, D. C.; Tandon, S. S.; Tucker, B. J.; Smith, G. W. Crystal structures and magnetic behaviour of the two forms of tetra-n-butylammonium tetraisothiocyanatochromate(II). *J. Chem. Soc., Dalton Trans.* **1994**, No. 9, 1425.
(14) Böhland, H.; Härtung, H.; Baumeister, U.; König, G.; Matthäus, R. Preparation, characterization and crystal structure of $Na_4[Mn(NCS)_6]\cdot 13H_2O$. *Mikrochim. Acta* **1997**, *125* (1−4), 149−152.
(15) (a) Addison, A. W.; Butcher, R. J.; Homonnay, Z.; Pavlishchuk, V. V.; Prushan, M. J.; Thompson, L. K. The Hexakis(thiocyanato)-ferrate(III) Ion: a Coordination Chemistry Classic Reveals an Interesting Geometry Pattern for the Thiocyanate Ligands. *Eur. J. Inorg. Chem.* **2005**, *2005* (12), 2404−2408. (b) Muller, U. Die Kristallstrukur von Tetramethylammonium-hexaisothiocyanatoferrat-(III), $[N(CH_3)_4]_3[Fe(NCS)_6]$. *Acta Crystallogr.* **1977**, *33*, 2197−2201.
(16) Wood, J. S.; McMullan, R. K. Structure of potassium tetrakis(isothiocyanato)cobaltate(II) monohydrate nitromethane solvate, $K_2[Co(NCS)_4].H_2O.2CH_3NO_2$, at 120 K by neutron diffraction. *Acta Crystallogr. Sect. C: Cryst. Struct. Commun.* **1984**, *40* (11), 1803−1806.
(17) Xie, K. P.; Wu, S. G.; Wang, L. F.; Huang, G. Z.; Ni, Z. P.; Tong, M. L. A spin-crossover phenomenon in a 2D heterometallic coordination polymer with $[Pd(SCN)_4]^{2-}$ building blocks. *Dalton Trans.* **2021**, *50* (12), 4152−4158.
(18) Kobayashi, M.; Savard, D.; Geisheimer, A. R.; Sakai, K.; Leznoff, D. B. Heterobimetallic coordination polymers based on the $[Pt(SCN)_4]^{2-}$ and $[Pt(SeCN)_4]^{2-}$ building blocks. *Inorg. Chem.* **2013**, *52* (9), 4842−4852.
(19) Coker, N. L.; Bauer, J. A.; Elder, R. C. Emission energy correlates with inverse of gold-gold distance for various $[Au(SCN)_2]^-$ salts. *J. Am. Chem. Soc.* **2004**, *126* (1), 12−13.
(20) Preetz, W.; Fricke, H.-H. Trennung von bindungsisomeren Hexakis(thiocyanato-isothiocyanato)-Komplexen von Ruthenium(III) an Celluloseionenaustauschern. *Fresenius' J. Anal. Chem.* **1981**, *306*, 115−120.
(21) Villars, P.; Cenzual, K.; Daams, J.; Gladyshevskii, R.; Shcherban, O.; Dubenskyy, V.; Kuprysyuk, V.; Savysyuk, I. $[Co(NH_3)_6][Os(SCN)_6]$. In *Structure Types. Part 8: Space Groups (156) P3m1 − (148) R-3*; Landolt-Börnstein - Group III Condensed Matter, 2010; pp 722.
(22) Fricke, H. H.; Preetz, W. Darstellung und Charakterisierung von bindungsisomeren Hexakis-(thiocyanato-isothiocyanato)-rhodaten(III) und Di-μ-thiocyanato-N, S-octathiocyanatodirhodat-(III). *Z. Anorg. Allg. Chem.* **1983**, *507* (12), 12−22.
(23) Fricke, H. H.; Preetz, W. Darstellung und Charakterisierung von bindungsisomeren Hexakis(thiocyanato-isothiocyanato)-iridaten-(III) und einiger Chloro-, Cyano-pentarhodanoiridate(III). *Z. Anorg. Allg. Chem.* **1983**, *507* (12), 23−34.
(24) Preetz, W.; Peters, G.; Vogt, J.-U. ^{103}Rh- und ^{15}N-NMR-Untersuchungen an bindungsisomeren Hexakis(thiocyanato(N)-thiocyanato(S))-rhodaten(III). *Z. Naturforsch.* **1993**, *48b*, 348−352.
(25) (a) Coe, B. J.; Glenwright, S. J. Trans-effects in octahedral transition metal complexes. *Coord. Chem. Rev.* **2000**, *203*, 5−80. (b) Mochida, T.; Maekawa, S.; Sumitani, R. Photoinduced and Thermal Linkage Isomerizations of an Organometallic Ionic Liquid Containing a Half-Sandwich Ruthenium Thiocyanate Complex. *Inorg. Chem.* **2021**, *60* (16), 12386−12391. (c) Fereidoni, S.; Ghiasi, R.; Pasdar, H. Theoretical Study of the Solvent Effect on the Electronic and Vibrational Properties of $[CpFe(CO)_2(NCS)]$ and $[CpFe(CO)_2(SCN)]$ Linkage Isomers. *J. Struct. Chem.* **2018**, *59* (5), 1058−1066. (d) Hsieh, C. H.; Brothers, S. M.; Reibenspies, J. H.; Hall, M. B.; Popescu, C. V.; Darensbourg, M. Y. Ambidentate thiocyanate and cyanate ligands in dinitrosyl iron complexes. *Inorg. Chem.* **2013**, *52* (4), 2119−2124. (e) Kobayashi, A.; Fukuzawa, Y.; Chang, H. C.; Kato, M. Vapor-controlled linkage isomerization of a vapochromic bis(thiocyanato)platinum(II) complex: new external stimuli to control isomerization behavior. *Inorg. Chem.* **2012**, *51* (14), 7508−7519.
(26) González, R.; Barboza, N.; Chiozzone, R.; Kremer, C.; Armentano, D.; De Munno, G.; Faus, J. Linkage isomerism in the metal complex hexa(thiocyanato)rhenate(IV): Synthesis and crystal structure of $(NBu_4)_2[Re(NCS)_6]$ and $[Zn(NO_3)(Me_2phen)_2]_2[Re(NCS)_5(SCN)]$. *Inorg. Chim. Acta* **2008**, *361* (9−10), 2715−2720.
(27) (a) Semrau, M.; Preetz, W. Darstellung und Kristallstruktur von $(n\text{-}Bu_4N)_3[Ir(NCS)(SCN)_5]$. *Z. Anorg. Allg. Chem.* **1996**, *622* (11), 1953−1956. (b) Rohde, J. U.; Preetz, W. Kristallstruktur von $(Me_4N)_3[Ir(SCN)_6]$, Schwingungsspektrum und Normalkoordinate-nanalyse. *Z. Anorg. Allg. Chem.* **1998**, *624* (8), 1319−1323.
(28) Snow, M. R.; Boosma, R. F. The crystal structures and isomerization of the linkage isomers thiocyanato- and isothiocyanato-pentaamminecobalt(III) dichloride, $[Co(SCN)(NH_3)_5]Cl_2\cdot H_2O$, and $[Co(NCS)(NH_3)_5]Cl_2$. *Acta Crystallogr., Sect. B: Struct. Crystallogr. Cryst. Chem.* **1972**, *28* (6), 1908−1923.
(29) Wechwithayakhlung, C.; Packwood, D. M.; Harding, D. J.; Pattanasattayavong, P. Structures, bonding, and electronic properties of metal thiocyanates. *J. Phys. Chem. Solids* **2021**, *154*, No. 110085.
(30) Cliffe, M. J.; Keyzer, E. N.; Dunstan, M. T.; Ahmad, S.; De Volder, M. F. L.; Deschler, F.; Morris, A. J.; Grey, C. P. Strongly coloured thiocyanate frameworks with perovskite-analogue structures. *Chem. Sci.* **2019**, *10* (3), 793−801.
(31) Siebel, E.; Fischer, R. D. Polymeric $[(Me_3Sn)_3Rh(SCN)_6]$: A Novel "Super-Prussian-Blue" Derivative Containing the Nonlinear -SCN-Sn-NCS- Spacer. *Chem. - Eur. J.* **1997**, *3* (12), 1987−1991.
(32) Tabe, H.; Matsushima, M.; Tanaka, R.; Yamada, Y. Creation and stabilisation of tuneable open metal sites in thiocyanato-bridged heterometallic coordination polymers to be used as heterogeneous catalysts. *Dalton Trans.* **2019**, *48*, 17063−17069.
(33) Wrzeszcz, G.; Dobrzańska, L.; Wojtczak, A.; Grodzicki, A. Magnetostructural characterisation of the first bimetallic assemblies derived from the anionic building block $[Cr(NCS)_6]^{3-}$ $[M(en)_3]_n[\{M(en)_2\text{-}\mu\text{-}SCN\text{-}Cr(NCS)_4\text{-}\mu\text{-}NCS\}_{2n}]$ with M = Ni(II), Zn(II). *J. Chem. Soc., Dalton Trans.* **2002**, 2862−2867.
(34) Katz, M. J.; Ramnial, T.; Yu, H. Z.; Leznoff, D. B. Polymorphism of $Zn[Au(CN)_2]_2$ and its luminescent sensory response to NH_3 vapor. *J. Am. Chem. Soc.* **2008**, *130* (32), 10662−10673.
(35) Ovens, J. S.; Leznoff, D. B. Thermal Expansion Behavior of $M^I[AuX_2(CN)_2]$-Based Coordination Polymers (M = Ag, Cu; X = CN, Cl, Br). *Inorg. Chem.* **2017**, *56* (13), 7332−7343.
(36) Frisch, M. J.; Trucks, G. W.; Schlegel, H. B.; Scuseria, G. E.; Robb, M. A.; Cheeseman, J. R.; Scalmani, G.; Barone, V.; Petersson,

https://doi.org/10.1021/acs.inorgchem.3c02292
Inorg. Chem. XXXX, XXX, XXX−XXX

741 G. A.; Nakatsuji, H.; Li, X.; Caricato, M.; Marenich, A. V.; Bloino, J.;
742 Janesko, B. G.; Gomperts, R.; Mennucci, B.; Hratchian, H. P.; Ortiz, J.
743 V.; Izmaylov, A. F.; Sonnenberg, J. L.; Williams-Young, D.; Ding, F.;
744 Lipparini, F.; Egidi, F.; Goings, J.; Peng, B.; Petrone, A.; Henderson,
745 T.; Ranasinghe, D.; Zakrzewski, V. G.; Gao, J.; Rega, N.; Zheng, G.;
746 Liang, W.; Hada, M.; Ehara, M.; Toyota, K.; Fukuda, R.; Hasegawa, J.;
747 Ishida, M.; Nakajima, T.; Honda, Y.; Kitao, O.; Nakai, H.; Vreven, T.;
748 Throssell, K.; Montgomery, J. A., Jr; Peralta, J. E.; Ogliaro, F.;
749 Bearpark, M. J.; Heyd, J. J.; Brothers, E. N.; Kudin, K. N.; Staroverov,
750 V. N.; Keith, T. A.; Kobayashi, R.; Normand, J.; Raghavachari, K.;
751 Rendell, A. P.; Burant, J. C.; Iyengar, S. S.; Tomasi, J.; Cossi, M.;
752 Millam, J. M.; Klene, M.; Adamo, C.; Cammi, R.; Ochterski, J. W.;
753 Martin, R. L.; Morokuma, K.; Farkas, O.; Foresman, J. B.; Fox, D. J.
754 *Gaussian 16, rev. C.01*; Gaussian, Inc.: Wallingford, CT, 2016.
755 (37) Wadt, W. R.; Hay, P. J. Ab initio effective core potentials for
756 molecular calculations. Potentials for main group elements Na to Bi. *J.*
757 *Chem. Phys.* **1985**, *82* (1), 284−298.
758 (38) Hay, P. J.; Wadt, W. R. Ab initio effective core potentials for
759 molecular calculations. Potentials for K to Au including the outermost
760 core orbitals. *J. Chem. Phys.* **1985**, *82* (1), 299−310.
761 (39) Hay, P. J.; Wadt, W. R. Ab initio effective core potentials for
762 molecular calculations. Potentials for the transition metal atoms Sc to
763 Hg. *J. Chem. Phys.* **1985**, *82* (1), 270−283.
764 (40) Köckerling, M.; Willems, J. B. Crystal structure of
765 tetraphenylphosphonium thiocyanate, $(C_6H_5)_4P(SCN)$. *Z. Kristallogr.*
766 *- New Cryst. Struct.* **1999**, *214*, 460.
767 (41) Norbury, A. H.; Sinha, A. I. P. The Co-ordination Behaviour of
768 the Cyanate Group towards Palladium(II) and Platinum(II). *J. Chem.*
769 *Soc. A* **1968**, 1598−1603.
770 (42) Schmidtke, H.-H. About the Ahrland-Chatt-Davies Classi-
771 fication of Rhodium and Iridium into Type (a) or (b) Central Atoms.
772 *J. Am. Chem. Soc.* **1965**, *87* (11), 2522−2523.
773 (43) Vogt, J.-U.; Haeckel, O.; Preetz, W. Darstellung und
774 Kristallstruktur von Tetraphenylphosphonium-
775 Hexathiocyanatorhodat(III), $[P(C_6H_5)_4]_3[Rh(SCN)_6]$. *Z. Anorg.*
776 *Allg. Chem.* **1995**, *621* (6), 1033−1036.
777 (44) Guégan, F.; Tognetti, V.; Joubert, L.; Chermette, H.; Luneau,
778 D.; Morell, C. Towards the first theoretical scale of the trans effect in
779 octahedral complexes. *Phys. Chem. Chem. Phys.* **2016**, *18* (2), 982−
780 990.
781 (45) Mautner, F. A.; Abu-Youssef, M. A. M.; Goher, M. A. S.
782 Polymeric complexes of cadmium(II) bridged simultaneously by
783 tetradentate picolinato and μ(1,1)-azido or μ(N,S)-thiocyanato
784 anions. Synthesis and structural characterization of $[Cd(picolinato)(N_3)]_n$
785 and $[Cd(picolinato)(NCS)]_n$. *Polyhedron* **1997**, *16* (2), 235−
786 242.
787 (46) (a) Ptaszyński, B.; Skiba, E.; Krystek, J. Thermal decomposition
788 of alkali metal, copper(I) and silver(I) thiocyanates. *Thermochim. Acta*
789 **1998**, *319* (1−2), 75−85. (b) Ptaszyński, B.; Skiba, E.; Krystek, J.
790 Thermal decomposition of Bi(III), Cd(II), Pd(II) and Cu(II)
791 thiocyanates. *J. Therm. Anal. Cal.* **2001**, *65*, 231−239.
792 (47) Figlar, J. N.; Stanbury, D. M. Thiocyanogen as an intermediate
793 in the oxidation of thiocyanate by hydrogen peroxide in acidic
794 aqueous solution. *Inorg. Chem.* **2000**, *39* (22), 5089−5094.

https://doi.org/10.1021/acs.inorgchem.3c02292
Inorg. Chem. XXXX, XXX, XXX−XXX